

Subcarrier Pairwise Coding for Short-Haul L/E-ACO-OFDM

Binhuang Song, Bill Corcoran, *Member, IEEE*, Qibing Wang, Leimeng Zhuang, *Senior Member, IEEE* and Arthur J. Lowery, *Fellow, IEEE*

Abstract— Dispersion-induced power fading in intensity modulated direct-detection (IM/DD) systems degrades the higher frequency subcarriers’ signal qualities. In Layered/Enhanced ACO-OFDM, which is a spectrally efficient version of asymmetrically clipped optical OFDM (ACO-OFDM), the error propagation in the iterative decoding can further degrade performance, especially when a low bias current is used for the directly modulated laser. In this letter, we propose using pairwise coding within each layer to improve the bit error rate (BER). We transmitted ~5-Gbaud 16-QAM OFDM signals over a 19.8-km single mode fiber, and found a 3.6-dB improvement in the Q^2 -factor.

Index Terms— Direct modulation direct-detection (DM/DD), asymmetrically clipped orthogonal frequency division multiplexing (ACO-OFDM), optical communications, pairwise coding.

I. INTRODUCTION

Intensity modulation using directly modulated lasers (DML) with direct-detection receivers (IM/DD) is a compact technology suitable for pluggable transceivers for short-haul links. Unfortunately, directly modulated lasers have limited bandwidths, so the electrical spectral efficiency of the modulation format is important. Pulse amplitude modulation (PAM-4) provides twice the electrical spectral efficiency (SE) of on-off keying [1]. Discrete multi-tone (DMT), carrier-less amplitude and phase modulation (CAP) and optical OFDM are able to support M-QAM formats [1-3]. However, DMT and dc-biased optical OFDM (DCO-OFDM) require a large bias to map a bipolar signal onto a unipolar optical intensity modulated signal. Asymmetrically clipped optical OFDM (ACO-OFDM) is designed to reduce the bias to close to the laser’s threshold current to enable a stronger modulated (signal) power in proportion to the unmodulated power, but sacrifices half of the optical and electrical spectral efficiency [4]. Layered/Enhanced techniques regain ACO-OFDM’s spectral efficiency (L/E-ACO-OFDM) [5-8] and theoretically require the lowest optical powers for $SE > 3\text{bits/Hz}$. Similarly, enhanced-unipolar OFDM (EU-OFDM) [9], which is based on Flip OFDM [10], offers the same advantage, as does Augmented-PAM-DMT [11]. However, in IM/DD systems, the optical double-sideband

modulation (DSB) interacts with fiber dispersion to create strong nulls in the baseband frequency response, which will degrade the signal quality of the high-frequency subcarriers in L/E-ACO OFDM. Moreover, the low-bias also reduces the laser’s modulation bandwidth and introduces waveform distortion including chirp and turn-on jitter. As well as affecting Layer 1 of these systems (the ACO-OFDM layer), errors will propagate to the higher layers during the iterative decoding process [5].

The iterative decoding process starts from Layer 1 in L/E-ACO-OFDM, in which the clipping distortion falls on even frequency slots if the signal-bearing subcarriers are placed on odd-frequency slots [4]. To allow these even subcarriers to be used for higher layers, the receiver needs to cancel the clipping distortion generated by Layer 1. This is achieved by detecting the data as in a normal receiver, then recreating Layer 1’s clipped waveform using the same methods to those used in the transmitter. The recreated waveform is then subtracted from the received waveform. The signal of Layer 2 is then available, which uses subcarriers $4n-2$ ($n = 1, 2, \dots$), so that its clipping distortion falls on subcarrier slots $4n$. If Layer 2 is cancelled at the receiver, Layer 3 can use half of the subcarrier slots $4n$.

If the receiver recovers Layer 1’s symbols incorrectly, the cancellation process will be imperfect, and distortion will propagate to the higher layers, increasing their error rates. Because for the same level of noise higher-order modulation formats have more errors, the error propagation will reduce L/E-ACO-OFDM’s low-bias advantage for high spectral efficiency systems.

In this paper, we introduce the pairwise coding (PWC) technique to L/E-ACO-OFDM system. Pairwise coding has been demonstrated as an effective method to maximize the overall system performance when there is an imbalance in SNRs between two ‘channels’. This imbalance may due to uneven noise distribution in IM/DD OFDM, polarization dependent loss, inter-channel-interference in superchannel transmission systems and the imperfections of ROADMs filters [12-15]. Importantly, PWC adds no overhead at the pre-coding stage, is computationally-efficient to decode, and gives large performance gains for large SNR differences.

In this paper, we use a 19.8-km optical fiber transmission

This work is supported under the Australian Research Council’s Laureate Fellowship (FL130100041) scheme and CUDOS – ARC Centre of Excellence for Ultrahigh bandwidth Devices for Optical Systems (CE110001018).

Binhuang Song, Bill Corcoran, Qibing Wang, Leimeng Zhuang and Arthur Lowery are with the Electro-Photonics Laboratory, Dept. of Electrical and

Computer Systems Engineering, Monash University, Clayton, VIC 3800, Australia. (e-mail: binhuang.song@monash.edu; bill.corcoran@monash.edu; qibing.wang@monash.edu; leimeng.zhuang@monash.edu; arthur.lowery@monash.edu).

experiment, we show that using PWC can improve L/E-ACO-OFDM, with only a slightly increased computational complexity. The error propagation was decreased due to the reduced number of error bits in the lower layers. Our experimental results shows a 3.6-dB improvement in Q^2 -factor for ~5-Gbaud 16QAM. Compared with our previous papers, in this work, we implemented PWC for 16QAM, which does not have a closed-form expression for optimal angle as does QPSK. Secondly, we show that applying PWC within each layer can improve the system performance in L/EACO-OFDM for short-haul transmission link. This work highlights the advantage of using PWC in spectrally-efficient formats where iterative decoding is used [9, 11].

II. PAIRWISE CODING FOR L/E-ACO

The idea of pairwise coding for a pair of unequal-SNR subcarriers is that the noise imbalance is transferred to the inphase and (I) and quadrature (Q) components of both subcarriers. Because of the ‘waterfall effect’ of BER versus SNR, the overall BER performance can be improved.

A. Pairwise coding for 16QAM

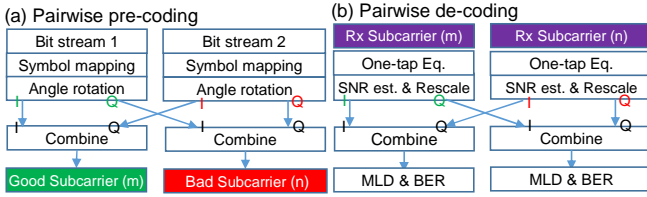


Fig. 1. (a) Pre-coding and de-coding. (b) Process for pairwise coding.

We explain the procedure of pairwise pre-coding and de-coding for 16QAM. Figure 1(a) shows the pairwise pre-coding process between two subcarriers. Similar to [12], bit-to-symbol mapping to firstly generate M -QAM symbol streams. Then, two symbol streams are rotated by an angle, θ_k , which is calculated to minimize the overall BER of each pair of subcarriers. The optimal angle for the k^{th} -pair with SNR_i and SNR_j for a general M -QAM constellation is given by [16]:

$$\theta_k(\lambda_{i_k}, \lambda_{j_k}) = \arg \max_{\theta_k \in [0, 2\pi]} \left(\min_{(p, q) \in S_M} (d_k^2(p, q, \theta_k)) \right) \quad (1)$$

where the target function d_k^2 is defined as:

$$d_k^2(p, q, \theta_k) = (p^2 + q^2) \left\{ SNR_{i_k} \cos^2 \left(\theta_k - \tan^{-1} \left(\frac{q}{p} \right) \right) + SNR_{j_k} \sin^2 \left(\theta_k - \tan^{-1} \left(\frac{q}{p} \right) \right) \right\} \quad (2)$$

As shown in Eq. (1), to find the optimal angle we need to test each candidate θ_k for a combination of (p, q) in set S_M , which is defined as:

$$S_M = \left\{ (p, q) \mid |p|, |q| \in [0, (\sqrt{M} - 1)], (p, q) \neq (0, 0) \right\} \quad (3)$$

In our experiment, we chose to implement 16-QAM (i.e. $M=16$). After angle rotation, the in-phase and quadrature parts are interleaved between high-SNR (good) and low-SNR (bad) subcarriers and then combined before an inverse discrete Fourier transform (DFT).

Figure 1(b) illustrates de-coding process. Using a training

sequence, one-tap equalization is performed and SNRs are estimated for all subcarriers. Then the I and Q components of the equalized symbols are rescaled by multiplying the square-roots of their SNRs. After in-phase and quadrature part are de-interleaved, a symbol-by-symbol slicer-like maximum-likelihood detection (MLD) is used to make the symbol decisions, D_s :

$$D_s = \arg \min_{C_k} \left\{ |E_s - T_k|^2 \right\} \quad (4)$$

$$T_k = \Re \left(C_k e^{j\theta} \right) \sqrt{SNR_{good}} + j \Im \left(C_k e^{j\theta} \right) \sqrt{SNR_{bad}}$$

where: E_s is the rescaled received signal, T_k is the rotated and scaled referencing points from conventional M -QAM constellation points, C_k . Without PWC, $\theta=0$, $SNR_{good}=SNR_{bad}$, and so $T_k=C_k$. Finally the error bits can be detected and BER is calculated for evaluating the system performance.

B. Pairing scheme for L/E-ACO-OFDM

The performance of L/E-ACO-OFDM depends on the correct decoding of the lower layers, because of the iterative decoding process used to reveal the higher layers [5]. More error bits in lower layers will introduce many incorrect estimations of clipping noise, therefore, resulting in imperfect cancellation of the lower layer’s clipped signal, leading to error propagation into the higher layers. Clipping noise from one subcarrier in a lower layer will introduce noise into multiple frequencies in a higher layer, which can be clearly seen from a half-wave-rectified (i.e. zero-clipped) sine wave ($f(t)=\sin(\omega_0 t)$), as:

$$f_{rec}(t) = \frac{A}{\pi} + \frac{A}{2} \sin \omega_0 t - \frac{2A}{\pi} \sum_{n=1}^{\infty} \frac{\cos(2n\omega_0 t)}{4n^2 - 1} \quad (5)$$

Conversely, one subcarrier in a higher layer is affected by the clipping noise estimation errors from multiple subcarriers in a lower layer. That is, the distortion of subcarriers in different layers will not be independent, so pairing them is not beneficial. Therefore, we will always pair subcarriers from the same layer. Fortunately, the number of bit errors in one layer can be reduced using pairwise coding, thus the clipping noise estimation and cancellation will be more accurate. Thus, error propagation to higher layers can be mitigated.

III. EXPERIMENTS

We experimentally examined PWC for L/E-ACO-OFDM in a 19.8-km standard single-mode fiber IM/DD link.

A. Experimental setup

To fairly demonstrate the performance improvement when using PWC, we used the same setup for the OFDM signal with or without PWC, which is shown in Fig. 2(a). The transmitted L/E-ACO-OFDM consists of 4 layers, carrying 45, 22, 11 and 6 subcarriers. The drive signal was generated offline in MATLAB with a 1024-FFT with 32-point cyclic prefix (CP). The sample rate was 60.09 Gsample/s, giving $(60.09/1024 \times (45+22+11+6)) = 5$ Gbaud. A Tektronix 7102 arbitrary waveform generator (AWG) and amplifier were used to drive a laser with a 1.59-V (peak-to-peak) signal. Because of the total 50- Ω impedance of the laser and series resistor, the current swing was 31.8 mA (peak-to-peak). The laser is a Gooch & Housego AA0701 DFB (threshold current = 13 mA),

and was biased at 29 mA and controlled to 25 °C. The output power is 2.7 dBm.

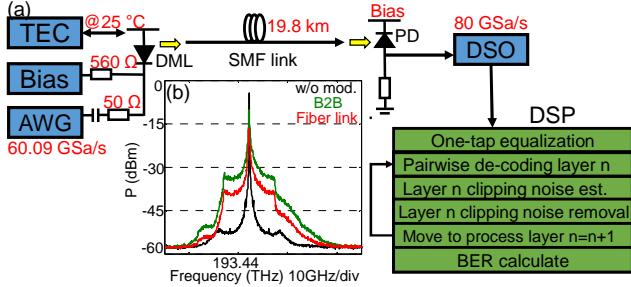


Fig. 2. (a) Experimental setup. DSP: off-line digital single processing. AWG: arbitrary waveform generator. DML: direct modulated laser. TEC: temperature controller. SMF: single mode fiber. PD: photodetector. DSO: digital oscilloscope. (b) Measured optical spectra.

At the receiver, a 40-GHz photodiode fed a 28-GHz real-time digital oscilloscope (Agilent DSO-X92804A), sampling at 80 GSamples/s. Figure 2(b) are measured optical spectra (black) without modulation, (green) the back-to-back received signal, (red) after the link. The asymmetry of each modulated spectrum is due to the complex dynamics of the laser under direct modulation. The receiver DSP flow with pairwise decoding is also shown in Fig. 2. The receiver DSP without PWC can be obtained by simply removing the de-coding step [17].

B. Channel SNRs and optimal angle searching for PWC

To determine the optimal rotation angles, we firstly obtained the SNRs for each subcarrier using a DCO-OFDM signal comprising 89 subcarriers with the same per-subcarrier bandwidth as the L/E-ACO-OFDM signal. We did not use an L/E-ACO-OFDM signal here because of the interdependence of its subcarriers, which would muddle the results. As the outputs of directed-modulated DFB lasers are double-sideband intensity modulated signals, dispersion-induced power fading will be observed after transmitting an optical fiber. The chirp of the directly modulated laser will affect power fading frequency point compared with an externally modulated DSB signal. In

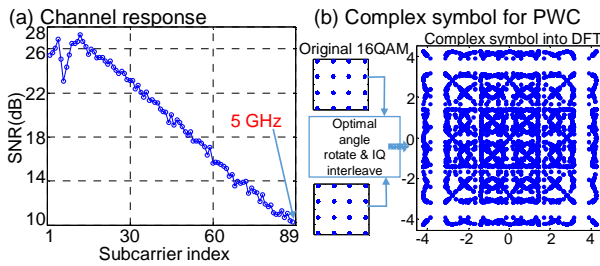


Fig. 3: (a) SNR versus channel index. (b) Complex symbol constellations after optimal angle rotation for PWC for all subcarriers.

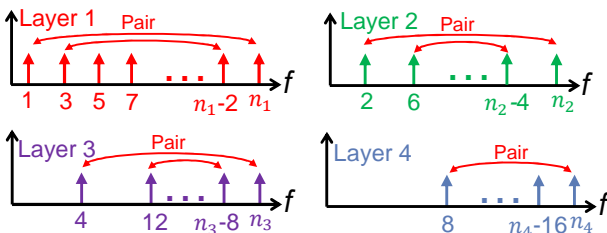


Fig. 4: Suitable pairing schemes for each layer of L/E-ACO-OFDM.

Fig. 3, except for the lowest-frequency subcarriers, the SNRs monotonically reduce at higher frequencies.

Based on these SNR results, a suitable pairing scheme for L/E-ACO-OFDM is shown in Fig. 4. This pairs the low-SNR subcarriers with high-SNR subcarriers. Layer 1 pairs 44 subcarriers (giving 22 pairs), 2 pairs 22, 3 pairs 10, and 4 pairs 6 subcarriers. Then, by utilizing Eq. (1), optimal angles are found. The angle searching precision was set at 0.5° to save computation. Figure 3(b) shows the constellation after IQ interleaving, which is then sent to the IDFT.

IV. RESULTS AND DISCUSSION

We first transmitted the L/E-ACO-OFDM signal without pairwise coding; the BERs for all subcarriers are shown in Fig. 5(a). In Layer 1 (circles), half of the subcarriers had no errors; the higher frequency subcarriers had more errors, which is consistent with the measured channel quality that was shown in Fig. 3(a). The 2nd (triangles) 3rd (diamonds) and 4th (squares) layers have descending performance, because the erroneous bits in the *n*th layer introduces errors into the (*n*+1)th, (*n*+2)th... layers. As discussed, the error propagation spreads across many frequencies, such that an error in say Layer 1 of Subcarrier 41 may increase the error probability in many subcarriers of Layer 2. This is evidenced in Fig. 5(a) where errors appear at the low-frequency subcarriers of Layer 2; obviously these errors do not come from the low-frequency subcarriers of Layer 1 as they had no errors, so Layer 2’s errors must have come from the higher-frequency subcarriers of Layer 1.

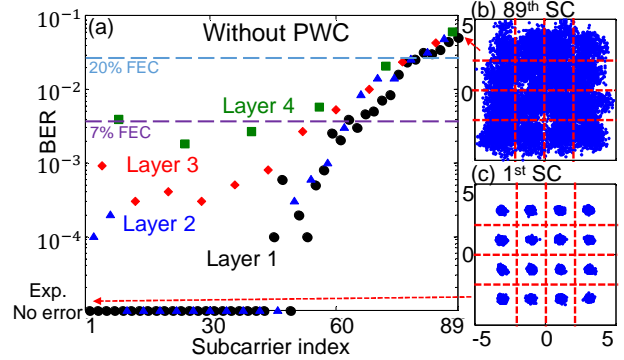


Fig. 5. Results without PWC. (a) Measured BERs. Received symbol constellations after rescaling for: (b) 89th subcarrier. (c) 1st subcarrier. Red dashed lines: decision thresholds.

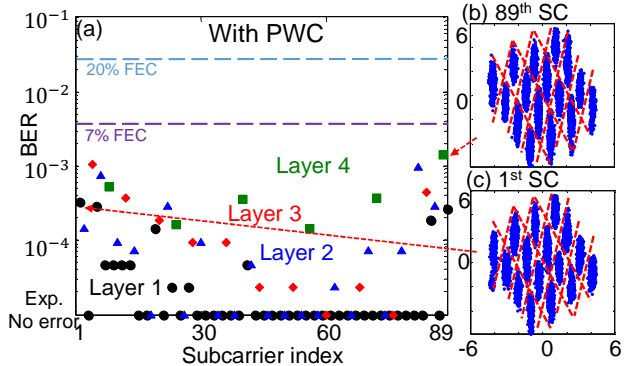


Fig. 6. Results with PWC. (a) Measured BERs. Received symbol constellations after rescaling for: (b) 89th subcarrier. (c) 1st subcarrier. Red dashed lines: decision thresholds.

Figure 6(a) shows the results when pairwise coding is used. The high-index subcarriers improved the most, as they benefitted from pairing a low-frequency subcarrier with a high-frequency subcarrier. In general, middle-index subcarriers have better performance than that of either low- or high-index subcarriers. This is due to the pairing scheme—the overall constellation spread is larger for low- and high-index subcarrier pairs than two middle-index subcarrier pairs. Although some error bits appeared in low-index subcarriers, their performance is still acceptable with 7% FEC overhead. The rescaled received signal constellations are plotted in Figs. 6(b) and 6(c), for the 1st and 89th subcarriers. The IQ de-interleaving and scaling transfers the SNR imbalance between a pair of subcarriers to an IQ signal strength difference, generating elliptically-shaped symbols. The error rate is optimized by using maximum-likelihood detection; the decision thresholds are indicated by red dashed lines.

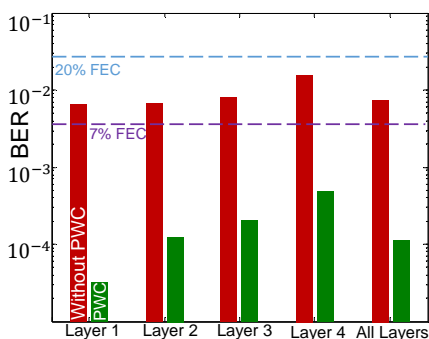


Fig. 7. BERs for each layer with and without PWC.

Figure 7 compares the BERs with and without PWC; there are fewer errors in the higher layers when PWC is used. Without PWC, all layers fail at 7% FEC: in contrast, no layer fails at 7% FEC after PWC. This translates to an overall benefit in error rate, for a small computational cost. Without PWC the BER over 3,578,400 bits was $<7.6 \times 10^{-3}$ for all subcarriers: with PWC, the BER improved to better than 1.14×10^{-4} . Equivalently, the Q^2 -factor, where $Q^2(\text{dB}) = 20 \log_{10}(\sqrt{2} \operatorname{erfc}^{-1}(2 \cdot \text{BER}))$ improved from 7.7 dB to 11.3 dB. Furthermore, in Fig. 5, differences in the overall BERs of the different layers are an indicator of error propagation (also as Fig. 7 in [5]): these differences are reduced in Fig. 6.

It is clear the PWC is aiding the high-frequency subcarriers by pairing them with lower-frequency subcarriers. An alternative strategy would be to use bit- and power-loading algorithms [18], to place more data onto the low-frequency subcarriers and balance SNRs. However, from a computational complexity point of view, the design of bit and power loading algorithm still requires multiple iterations to converge (e.g. computational complexity is $O(N \log N)$ for [18]), which is more complex than the non-recursive PWC method. Furthermore, the choice of modulation format in bit-loading algorithm requires more communication between the transmitter and receiver than pairwise coding, which only communicates SNRs to the transmitter to adjust the rotation angles. A full investigation of the performance of the two schemes is underway. A FEC gain-sharing method [19] can also reduce the number of error bits at the bit-decision level rather than symbol-decision level. By

mixing bit streams from two channels in the decoder matrix, the bit stream with good performance will cover the bad one through sharing the parity frame.

V. CONCLUSION

By pairing good and bad subcarriers within each layer, we have shown that the BER can be reduced for L/E-ACO-OFDM signals. A 3.6-dB improvement in Q^2 -factor was observed after 19.8-km single mode fiber transmission with ~5-Gbaud 16QAM using direct modulation and direct detection. The propagation of errors between layers was mitigated, due to the reduced number of errors in the higher layers.

REFERENCES

- [1] K. Zhong *et al.*, "Experimental study of PAM-4, CAP-16, and DMT for 100 Gb/s short reach optical transmission systems," *Opt. Express*, vol. 23, no. 2, pp. 1176-1189, 2015.
- [2] S. C. J. Lee *et al.*, "PAM-DMT for intensity-modulated and direct-detection optical communication systems," *IEEE Photon. Technol. Lett.*, vol. 21, no. 23, pp. 1749-1751, 2009.
- [3] M. I. Olmedo *et al.*, "Towards 400GBASE 4-lane solution using direct detection of MultiCAP signal in 14 GHz bandwidth per lane," in *Proc. OFC*, Anaheim, USA, 2013, PDP5C-10.
- [4] J. Armstrong and A. J. Lowery, "Power efficient optical OFDM," *Electron. Lett.*, vol. 42, no. 6, pp. 370-372, 2006.
- [5] A. J. Lowery, "Comparisons of spectrally-enhanced asymmetrically-clipped optical OFDM systems," *Opt. Express*, vol. 24, no. 4, pp. 3950-3966, 2016.
- [6] Q. Wang *et al.*, "Layered ACO-OFDM for intensity-modulated direct-detection optical wireless transmission," *Opt. Express*, 23(9), pp. 12382-12393 (2015).
- [7] M. S. Islam, D. Tsonev and H. Haas, "On the superposition modulation for OFDM-based optical wireless communication," in *Proc. GlobSIP*, Orlando, USA, 2015, pp. 1022-1026.
- [8] L. Chen, B. Krongold and J. Evans, "Successive decoding of anti-periodic OFDM signals in IM/DD optical channel," in *Proc. ICC*, Cape Town, South Africa, 2010, pp. 1-6.
- [9] D. Tsonev, S. Videv and H. Haas, "Unlocking spectral efficiency in intensity modulation and direct detection systems," *IEEE J. Sel. Areas in Comm.*, vol. 33, no. 9, pp. 1758-1770, 2015.
- [10] N. Fernando, Y. Hong and E. Viterbo, "Flip-OFDM for Unipolar Communication Systems," *IEEE Trans. Comm.*, vol. 60, no. 12, pp. 3726-3733, 2012.
- [11] M. S. Islam and H. Haas, "Augmenting the spectral efficiency of enhanced PAM-DMT-based optical wireless communications," *Opt. Express*, vol. 24, no. 11, pp. 11932-11949, 2016.
- [12] C. Zhu, *et al.*, "Improved polarization dependent loss tolerance for polarization multiplexed coherent optical systems by polarization pairwise coding," *Opt. Express* vol. 23, no. 21, pp. 27434-27447, 2015.
- [13] Y. Hong, A. J. Lowery, and E. Viterbo, "Sensitivity improvement and carrier power reduction in direct-detection optical OFDM systems by subcarrier pairing," *Opt. Express*, vol. 20, no. 2, pp. 1635-1648, 2012.
- [14] C. Zhu *et al.*, "Subband pairwise coding for robust Nyquist-WDM superchannel transmission," *J. Lightwave Technol.* Vol. 34, no. 8, pp. 1746-1753, 2016.
- [15] C. Zhu *et al.*, "Doubling the ROADM sites using pairwise coding for 4%-guard-band superchannels," in *Proc. OFC*, Anaheim, USA, 2016, Th1D.1
- [16] S. K. Mohammed *et al.*, "MIMO Precoding With X- and Y-Codes," *IEEE Trans. Inf. Theory*, vol. 57, no. 6, pp. 3542-3566, 2011.
- [17] B. Song *et al.*, "Experimental Layered/Enhanced ACO-OFDM Short-Haul Optical Fiber Link," *IEEE Photon. Technol. Lett.*, vol. 28, no. 24, pp. 2815-2818, 2016.
- [18] B. Krongold *et al.*, "Computationally efficient optimal power allocation algorithms for multicarrier communication systems." *IEEE Trans. Comm.*, vol. 48, no. 1, pp. 23-27, 2000.
- [19] J. Rahn *et al.*, "Transmission Improvement through Dual-Carrier FEC Gain Sharing", in *Proc. OFC*, Anaheim, USA, 2013, OW1E.5